Supporting Information File

Lepidocrocite-type Titanate Formation from Isostructural Prestructures under Hydrothermal Reactions: Observation by Synchrotron X-ray Total Scattering Analyses

Satoshi Tominaka,[†,§,*] *Hiroki Yamada*,[‡,§] *Satoshi Hiroi*,[#,§] *Saori I. Kawaguchi*,[§] *and Koji Ohara*[§]

†International Center for Materials Nanoarchitectonics (WPI-MANA), National Institute for Materials Science (NIMS), 1-1 Namiki Tsukuba, Ibaraki 305-0044, Japan.
§Research and Utilization Division, Japan Synchrotron Radiation Research Institute, 1-1-1 Kouto, Sayo-gun, Hyogo 679-5198, Japan.
‡Department of Chemical System Engineering, The University of Tokyo, 7-3-1 Hongo, Bunkyo, Tokyo 113-8656, Japan.
#Synchrotron X-ray Station at SPring-8, Research Network and Facility Services Division, National Institute for Materials Science (NIMS), 1-1-1 Koto, Sayo, Hyogo 679-5148, Japan.

Contents

1. TG-DTA
2. FTIR
3. XRD simulation for the crystalline product
4. Overview of the *in situ* X-ray total scattering measurements
5. Additional *in situ* X-ray total scattering data
6. Pictures of the solution
7. Relative PDF data
8. PDF curve fitting and simulation results
9. Details of data processing
10. Structural information data

Additional data

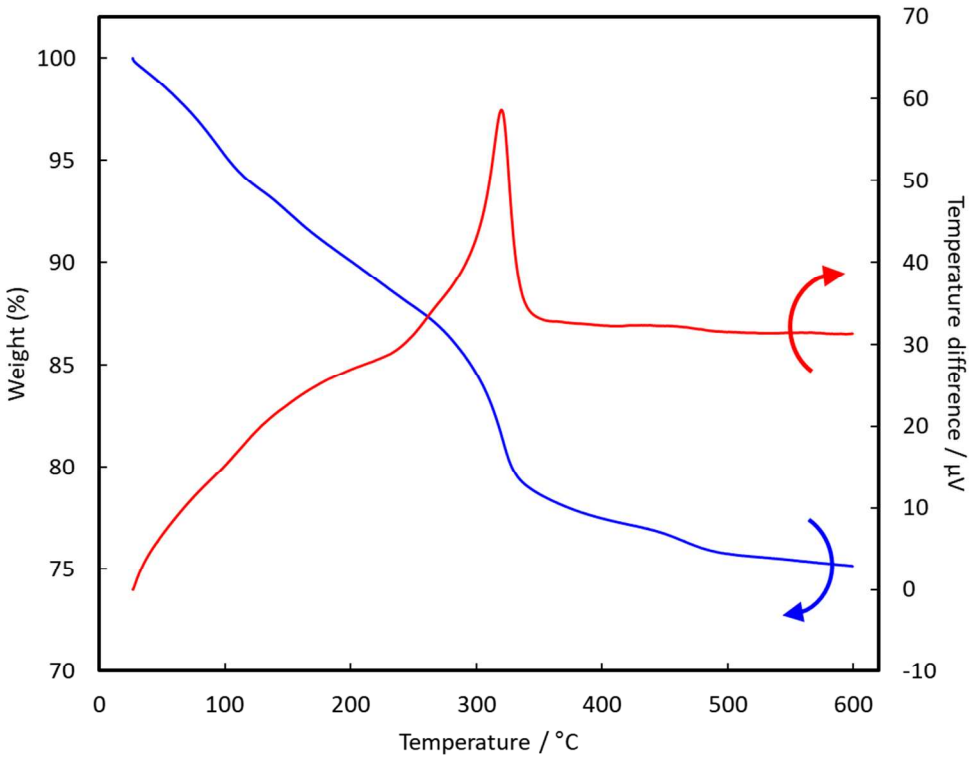

Figure S1 Simultaneous thermogravimetric analysis and differential thermal analysis (TG-DTA) performed at 5 °C min^{-1} in air. The weight losses are assigned to H_2O (RT to 120°C, 6.2 wt% loss), H_2O (120 to 230°C, 5.0 wt% loss) and tmah (230 to 405°C, 11.4 wt% exothermic loss). Note that another loss (2.2 wt%) was observed from 420°C to 600°C, which is attributed to the deoxygenation of excess O atoms located at the edge of sheets upon crystal structure transformation of the lepidocrocite-type TiO_2 into the anatase structure. Since the product formed during the TGA measurement is a yellow powder, the crystals are considered to contain oxygen vacancies, as often observed in titania crystals.

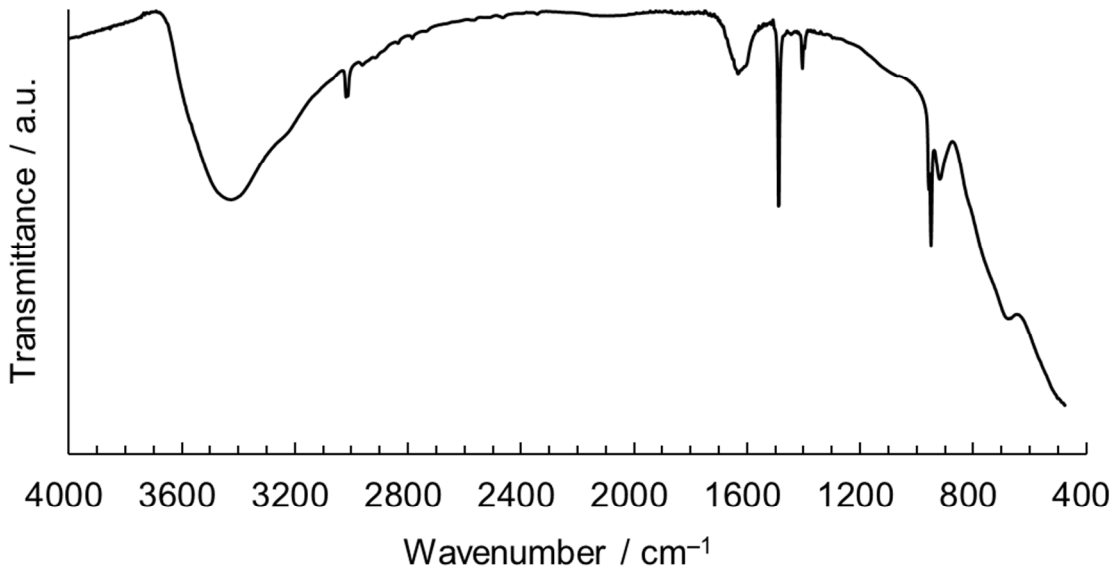

Figure S2 Fourier-transform infrared spectroscopy spectrum of the dried product (lepidocrocite-type titanate) measured in the transmission mode. The major peaks are assigned as 3426 cm^{-1} (broad, OH stretching), 3012 and 3020 cm^{-1} (CH stretching), 1628 and 1601 cm^{-1} (H–O–H bending), 1489, 1404, 947, 949 and 912 cm^{-1} (H–C–H bending), 1200–1000 cm^{-1} (broad CN stretching), 685 cm^{-1} (TiO stretching).

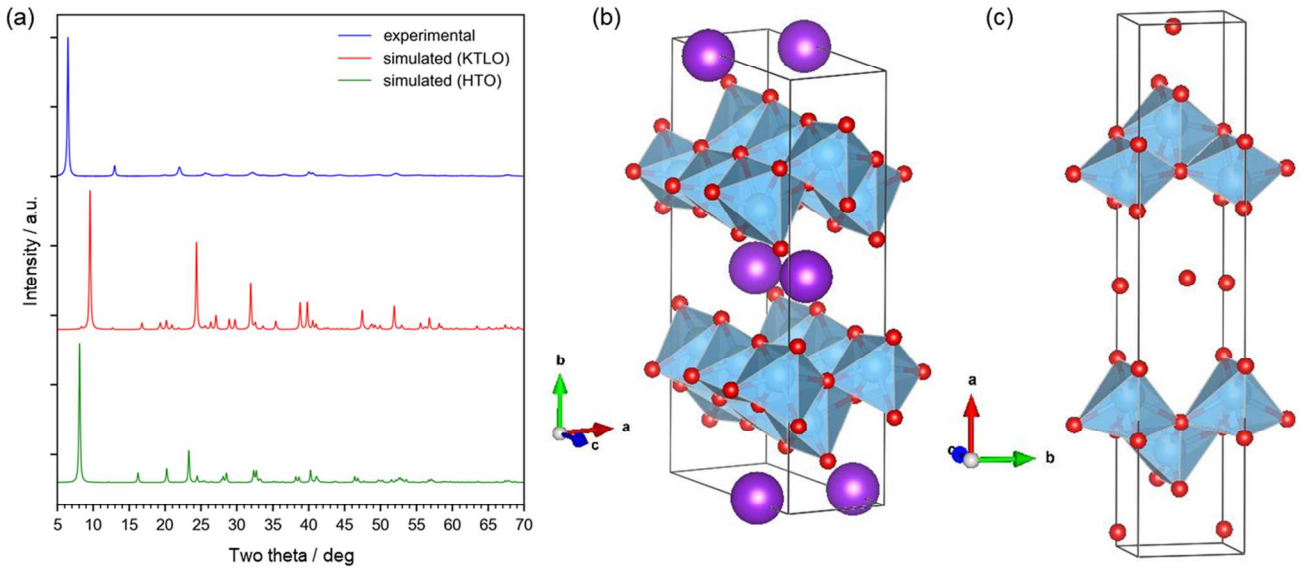

Figure S3 (a) XRD patterns used for the phase identification of $[TiO_2]\cdot nH_2O\cdot m((CH_3)_4N)$ (n = 0.54 and m = 0.22). Blue curve: experimentally obtained XRD. Red curve: simulated pattern for $K_{0.8}Ti_{1.73}Li_{0.27}O_4$ (KTLO). Green curve: simulated pattern for $H_{1.07}Ti_{1.73}O_4$ (HTO). The structure information files were obtained from the literature.[1] (b) Structure model of KTLO. (c) Structure model of HTO.

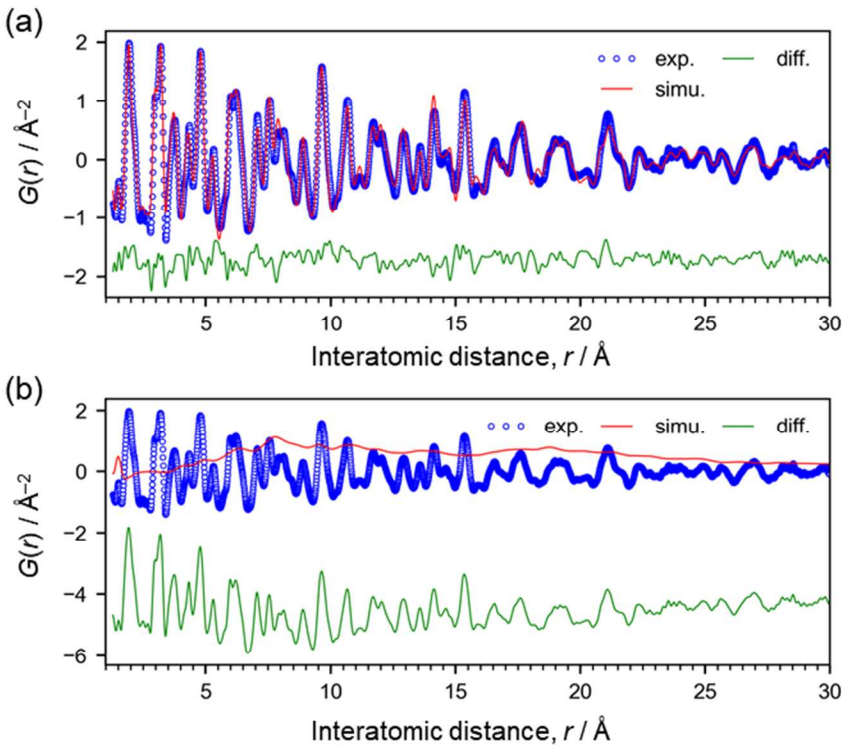

Figure S4 PDF fitting of the layered titanate crystals (λ = 0.1076 Å, Q = 1.6–29.0 Å^{-1}). (a) All atom pairs. (b) Partial PDFs for N-all and C-all pairs. For the simulation in the panel 'a', the fitting parameters were four lattice constants (a, b, c and β), the scale factor, a diameter, a sratio parameter for simulating short-range order within 1.7 Å, 29 parameters for the atomic coordinates of Ti and O atoms in the titanate under symmetry constraints, two U_{iso} parameters for the surface and core Ti, one U_{iso} parameter for O in the titanate and an occupancy value for the tmah molecules.

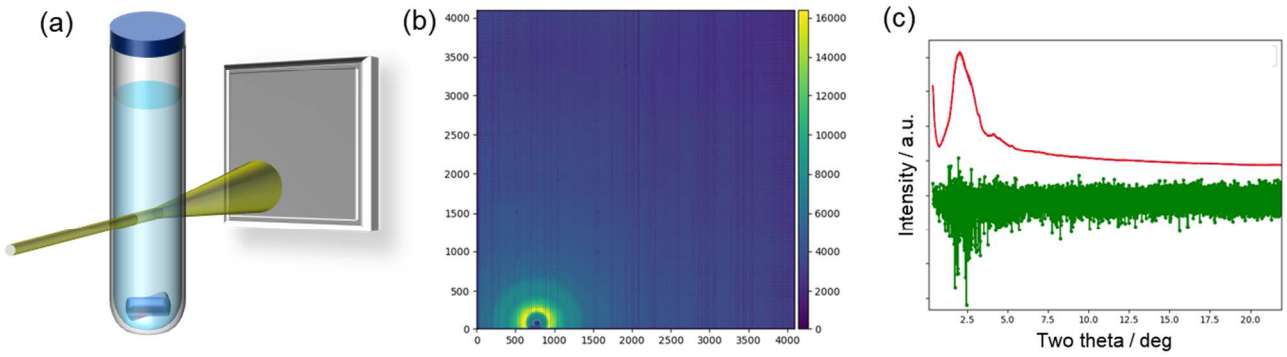

Figure S5 In situ X-ray total scattering measurements of the solution heated by microwaves. (a) Illustration showing the experimental setup. (b) Image data recorded on a flat panel detector. The direct beam position is at the bottom left. The vertical black lines are dead pixels, which were excluded using the PIXIA program. (c) One-dimensional data with and without noise filtering. The noise was removed as described in the analytical details. This data was obtained by our first in situ measurement under the hydrothermal conditions at BL08W, SPring-8. We then focused on reducing the noise, and thus the other diffraction image data reported in this paper had less noise.

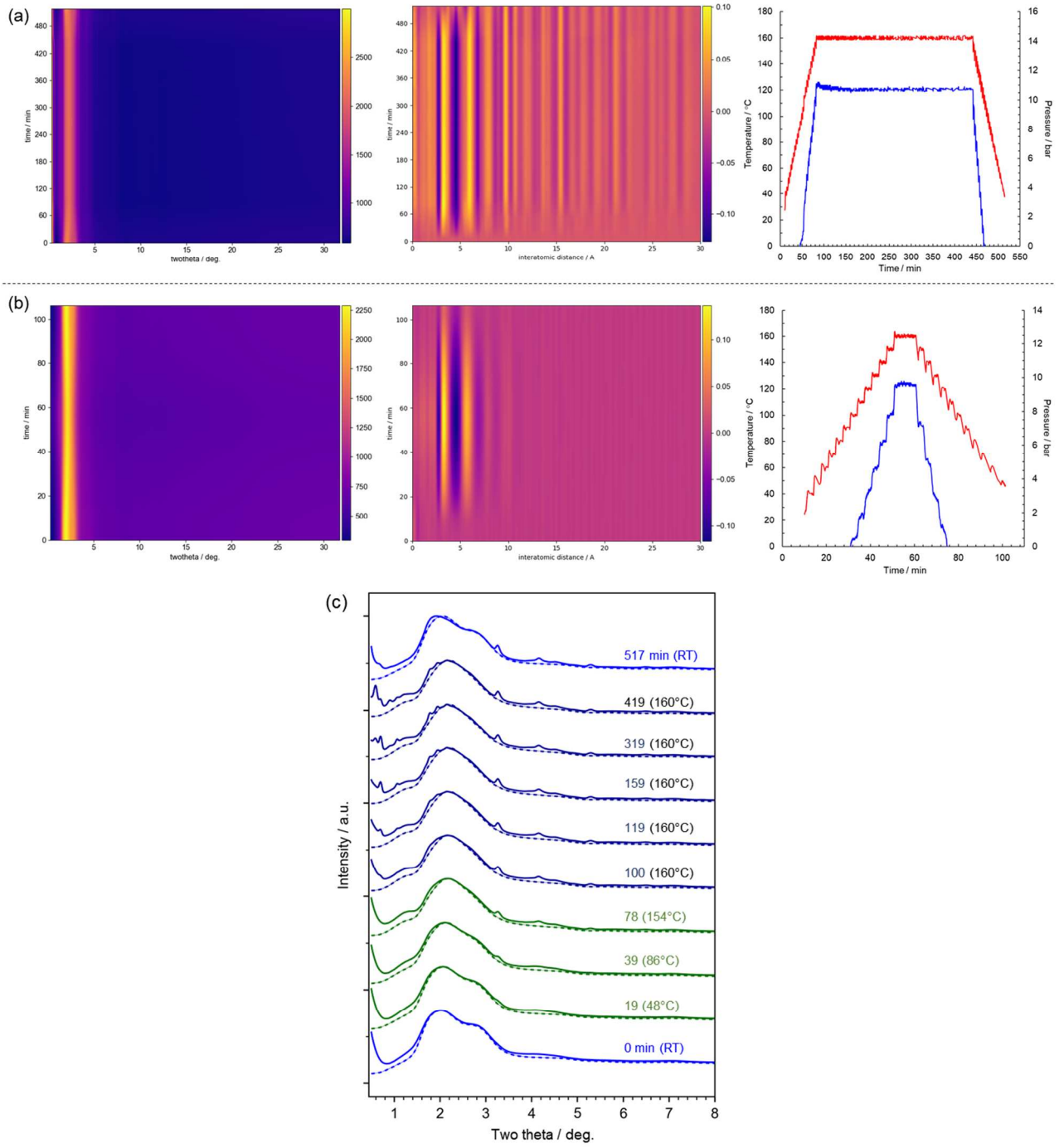

Figure S6 In situ X-ray total scattering experiments on the solution with titanate (a) and without titanate (b) (left: two theta; middle: relative PDF; right: temperature and pressure data). (c) Total scattering patterns at different temperatures (solid curves: data with titanate; dotted curves: data without titanate).

Figure S7 (a) Precursor solution immediately after the preparation. (b) Precursor solution left at RT for 1 h. The change in the appearance of the suspension is not accompanied by a structural change as found from the PDF data. Thus, this change is probably attributed to dissolution of the as-formed titanate structure. (c) Solution heated at 40°C for 1 min using the microwave reactor. (d) Solution heated at 160°C for 1 min using the microwave reactor.

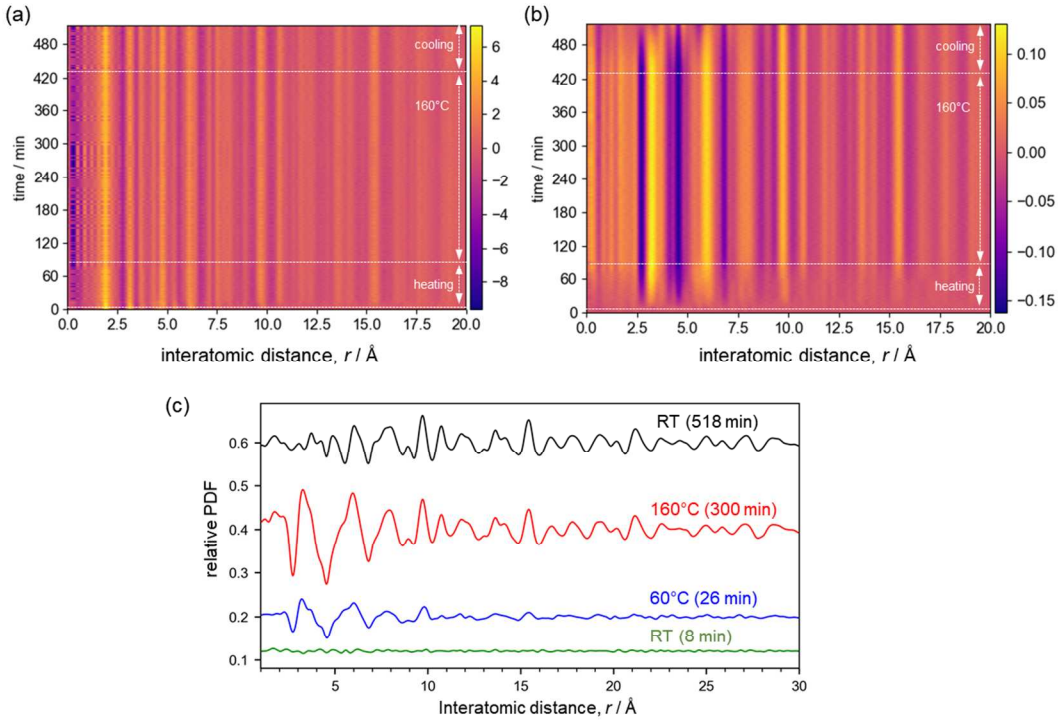

Figure S8 (a) Two-dimensional data of time-dependent reduced PDFs (same as Fig. 4a). (b) Relative PDF data. The scattering image data for the solution containing titanate (time = 0, RT) was subtracted from the other data and then normalized by a form factor calculated for the chemical composition of TiO_2 (Q range 0.8–15.0 Å^{-1}). This shows the structural change from the reference data. (c) Selected relative PDFs (Q_{max} = 15.2 Å^{-1}). This relatively low Q_{max} was only used for these relative PDFs.

The X-ray total scattering image data for the solvent only was subtracted from the image data for the solution containing titanate at each temperature, and then a 1D scattering pattern was obtained. After the data corrections (e.g., Compton scattering subtraction), the intensity data was normalized by a form factor calculated for the chemical composition of TiO_2 (Q range 0.0–18.0 Å^{-1}). Because these processes were automated and not optimized at each temperature, some of the $G(r)$ data have noise (or termination ripples) in the low r range. Thus, we could access these data after all the measurements. To monitor the structural changes during the synchrotron X-ray experiments, we used relative PDFs.

The relative PDFs were calculated by subtracting the initial total scattering data from the subsequent data and then normalized by the form factor calculated for the chemistry of TiO_2. The negative (darker) regions represent a decreased number of atom pairs compared with the initial data (time = 0 min), while the positive (brighter) regions mean an increased number of atom pairs. The positive regions

in the ranges of 3–4 Å and 5–6.5 Å suggest the formation of more Ti-Ti pairs in a layered structure, as found in the longer-range region as the thermal treatment proceeds. For example, even at 60°C, the features above 7 Å are almost the same as those in the PDF of the lepidocrocite structure, indicating the growth of lepidocrocite layered titanate.

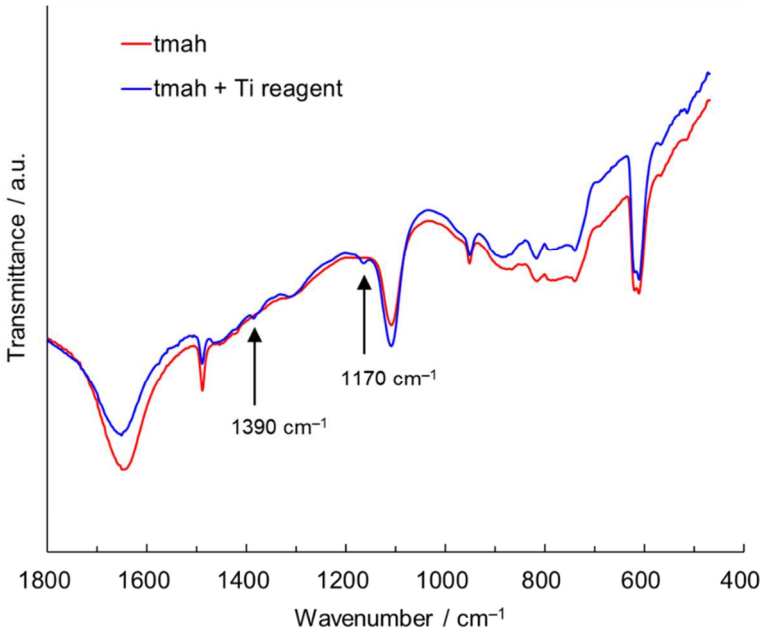

Figure S9 Fourier-transform infrared spectroscopy spectrum of the as-prepared solution compared with that of a solution of tmah in water. This data was collected in the attenuated total reflection configuration. The peaks observed in the solution containing the Ti reagent (Ti isopropoxide) are assignable to isopropanol.

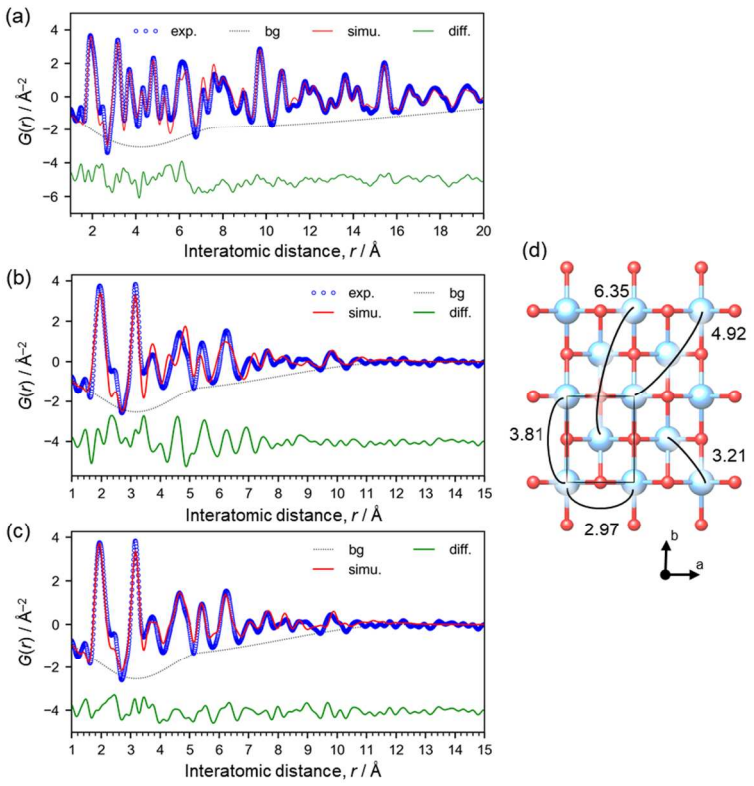

Figure S10 PDF curve-fitting results of the (a) titanate after the reaction measured at RT (fitting parameters were two lattice constants (*a* and *b*), the scale factor, the diameter, the sratio parameter for simulating short-range order within 3.46 Å, three parameters for the atomic coordinates of Ti and O atoms under symmetry constraints (*Pmmn*) and three U_{aniso} parameters for each site of one Ti site and two O sites); (b) titanate in the as-prepared solution simulated using the smaller model (fitting parameters were two lattice constants (*a* and *b*), the scale factor, the diameter, three parameters for the atomic coordinates of Ti and O atoms under symmetry constraints (*Pmmn*) and two U_{iso} parameters for Ti and O; and (c) titanate in the as-prepared solution simulated using the larger model (*P*1 space group, 2×2×1 supercell) (fitting parameters were two lattice constants (*a* and *b*), the scale factor, the diameter (fixed at 14.0 Å), two U_{iso} parameters for Ti (fixed at 0.0021 Å^2) and O (fixed at 0.0020 Å^2) and atomic coordinates for eight Ti sites and 16 O sites (changed under the restraints described in the main text)). The background curves or baselines were simulated using an empirical model described in the later section, "simulation of PDF using isolated cluster/nanosheet models" (panel 'a': *s1* = 1.20, *s2* = 7.89, *d* = 30.0 and *x* = 2.51; panel 'b' and 'c': *s1* = 2.30, *s2* = 5.33, *d* = 12.2 and *x* = 2.78). (d) Structure model showing Ti-Ti distances in the typical lepidocrocite structure observed along the *c* axis (blue: Ti; red: O).

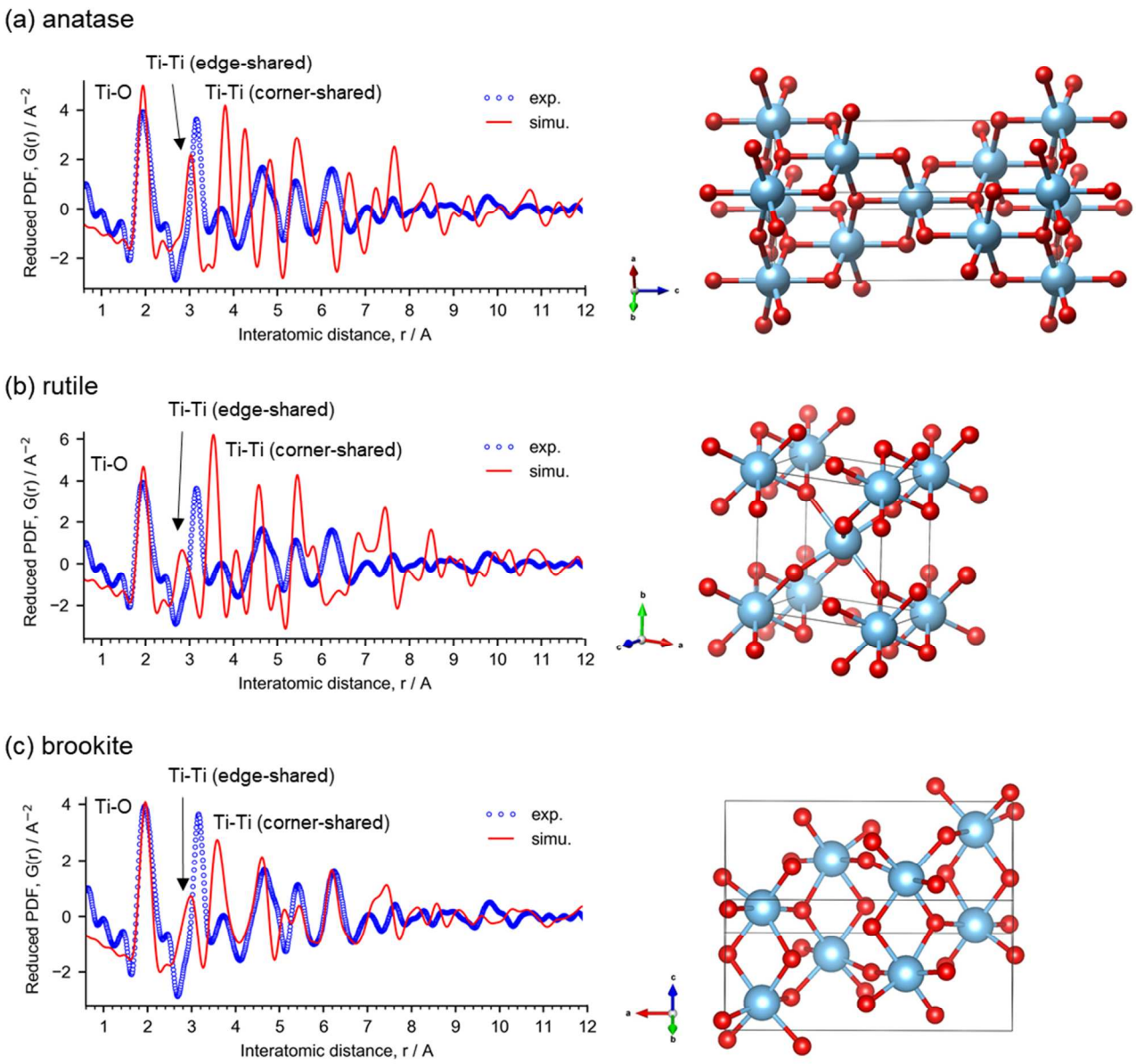

Figure S11 PDF curve-fitting results for the as-prepared solution using different structure models shown on the right (blue: Ti; red: O). Each experimental PDF (blue dots) was obtained from structure function in the range of Q = 0.972–18.921 Å^{-1}. (a) Structure of anatase TiO_2 (a = 3.7842, c = 9.5146; ICSD no. 9852). (b) Structure of rutile TiO_2 (a = 4.5941 Å, c = 2.9589 Å; ICSD no. 9161). (c) Structure of brookite TiO_2 (a = 9.174 Å, b = 5.449 Å, c = 5.138 Å; ICSD no. 36408).

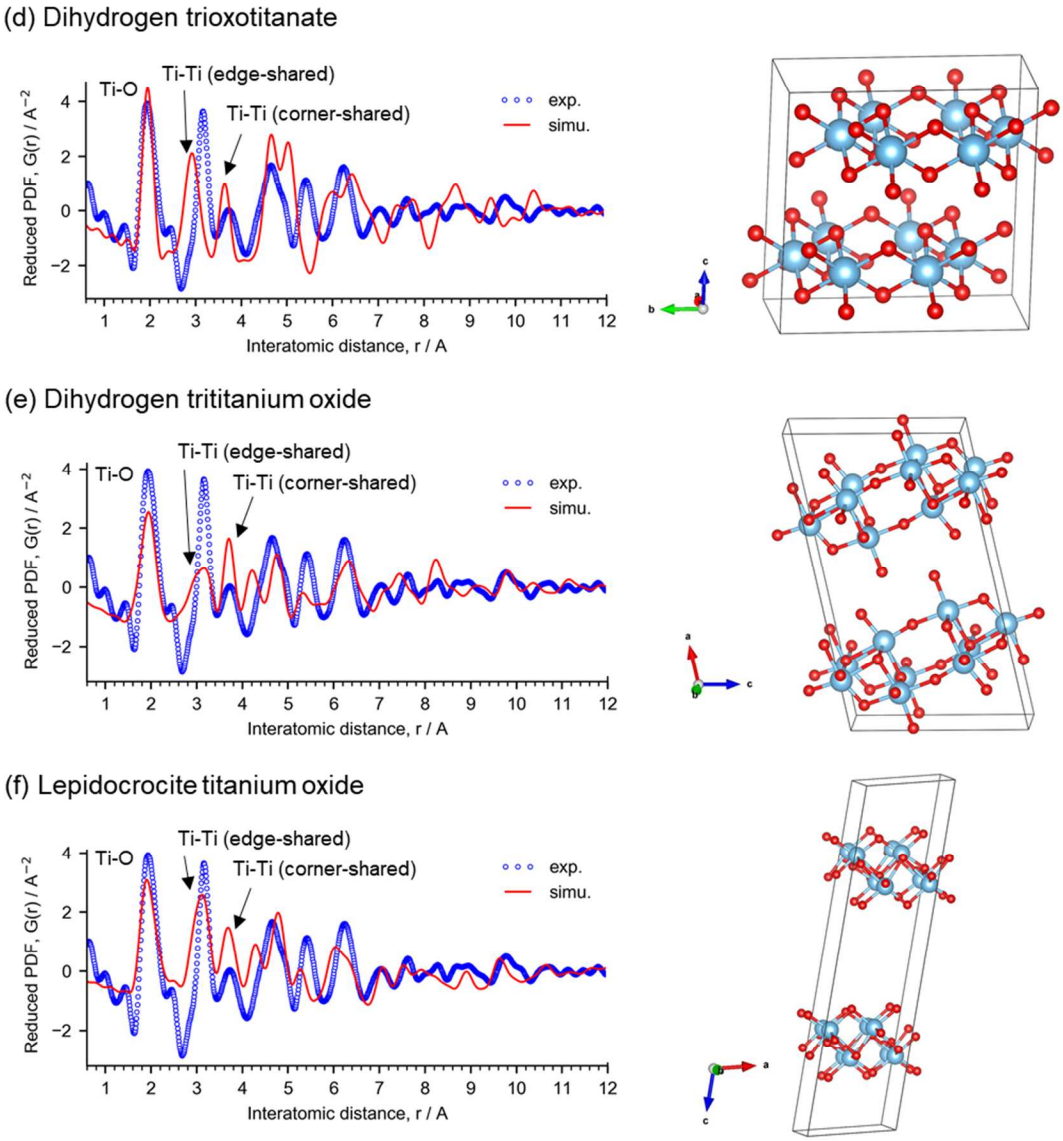

Figure S11 (continued) (d) Structure of dihydrogen trioxotitanate $H_2Ti_2O_3$ (a = 4.97 Å, b = 9.08 Å, c = 9.53 Å, β = 99.86°; ICSD no. 195648). (e) Structure of dihydrogen trititanium oxide $H_2Ti_3O_7$ (a = 4.97 Å, b = 9.08 Å, c = 9.53 Å, β = 99.86°; ICSD no. 195648). (f) Structure of lepidocrocite-type TiO_2 (a = 4.97 Å, b = 9.08 Å, c = 9.53 Å, β = 99.86°; solved in this work). Ti and O atoms were included, and other atoms were excluded from the simulation. U_{iso} = 0.005 Å^2 was used for all the atoms. A spherical particle with a diameter of 15 Å was used for all the models. A scale factor of 1.0 was used for all the calculations.

Details of data processing

Conversion of 2D data into 1D data using PIXIA program.

The conversion from 2D image data to a 1D scattering profile was performed using the PIXIA program. This program is being developed and will be available free of charge from National Institute for Materials Science (NIMS) (https://samurai.nims.go.jp/profiles/tominaka_satoshi?locale=en). The program is written in Python and has a graphical user interface prepared using the wxPython module. The current version of PIXIA is being tested by beta testers and will be publicly available soon. **Figure S12** shows the user interface. Details of the mathematical treatments in this program will be available in future, and here we summarize the key concepts and equations required for the work reported in this paper.

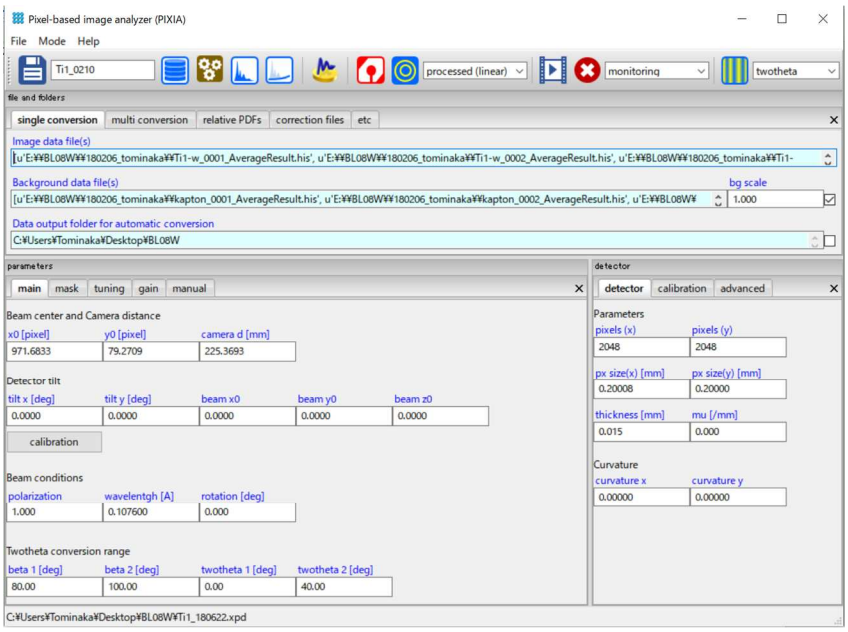

Figure S12 User interface of PIXIA program.

PIXIA stands for "Pixel-based Image Analyzer", and is dedicated to image processing in X-ray scattering experiments. Briefly, the program can extract scattering data through the noise filtration and data corrections required for X-ray scattering analysis such as polarization correction. We assume a 2D detector as an array of square-pillar

detectors, and the coordinates of each pixel are defined as those at its center as shown in **Figure S13**. The 2D data is a function of the physical space coordinates (x, y, z) or X-ray scattering coordinates (θ, β), where β is the angle in the circumferential direction (anticlockwise). After image processing and correction for the intensities recorded at each pixel, a data list of the corrected intensity, i_{cor}, vs θ is obtained. The histogram of i_{cor} vs θ has many data points (e.g., one million points for 1000×1000 pixels). A mathematical filter is used to obtain the scattering signal by removing the noise (note that current version of PIXIA uses a Savitzky–Golay filter).

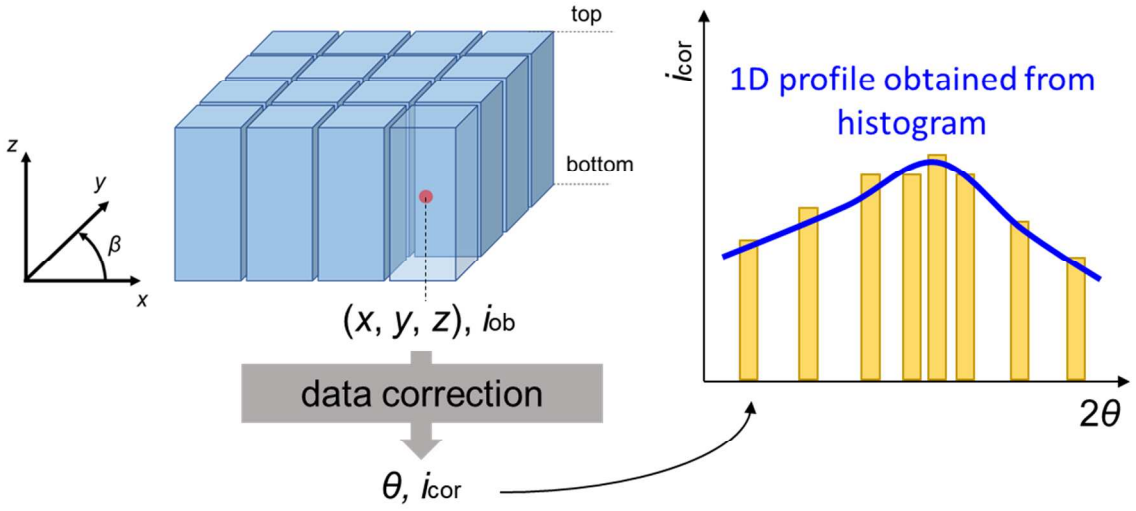

Figure S13 Concept of data processing in PIXIA.

In the data correction, the recorded intensities, I_{rec}, are corrected by removing offset values, I_{ofs}, and then normalized by the gain values G, to obtain observable intensities, I_{ob},

$$I_{ob}(x,y) = \left(I_{rec}(x,y) - I_{ofs}(x,y)\right) \cdot G(x,y). \qquad \text{(S1.1)}$$

The polarization effect, P, is corrected in accordance with the original equation written by Kahn et al.,[2] which requires more calculations than the modified equation used for some programs dedicated to XRD within the small-Q range. Then, the intensity of each pixel is normalized by the proportion of Debye–Scherrer rings recorded on the projected area of each pixel, D. The intensity of each pixel is further corrected for the oblique incidence of the X-ray to the detector having thickness h and absorption coefficient μ. Details of the mathematics will be available in future (e.g., in a manual).

$$I_{\mathrm{cor}}(x, y, z;\ \theta, \beta) = I_{\mathrm{ob}}(x, y) \cdot P(\theta, \beta) \cdot D(x, y, z) \cdot O(x, y, z, h, \mu) - I_n \qquad \text{(S1.2)}$$

The intensities still contain unavoidable noise, I_{n}, which contains statistical noise and other noises. The noise is not a function of the physical space coordinates (x, y, z) or the X-ray scattering coordinates (θ, β); thus, we can remove the noise from both coordinates. We excluded pixels (*i*) where G values are not constant (e.g., within 10% error) at different exposure times, (*ii*) where the intensities are markedly different from those of the surrounding pixels in the physical space coordinates (e.g., 50% error) and then (*iii*) where there are apparently different intensities (e.g., 50% error) compared with averaged intensities at each 2θ angle in the I vs 2θ graph. Then, intensity vs 2θ data is obtained using all the remaining pixel data.

Figure S14 shows an example of data conversion. **Figure S14a** shows the 2D data (NIST CeO_2) after subtracting the air background recorded under the same integration conditions. Parameters including angles, polarization and area correction factors were calculated as shown in **Fig. S14b**. Then, after masking the beam-stop region and dead pixels, the 2D data shown in **Fig. S14a** was converted into 1D profile shown in **Fig. S14c**. In the case of XRD, the profile shown in **Fig. S14c** is sufficiently accurate for data analysis. However, in the case of PDF analysis, the data still contains the fluorescence intensity and Compton scattering intensity as well as the effect of the modulated offset due to the exposure. As described above, the conversion of a 2D image into a 1D profile requires a complicated mathematical treatment, and thus even constant offset values remain in the data signals and the resultant 1D profile has a curved offset shape. For example, a dummy image having 100 counts at each pixel was converted into the 1D profile shown in **Fig. S14d** using the same parameters as those for CeO_2 data conversion. Thus, for the PDF analysis, we converted dummy image data having a constant intensity at each pixel into a 1D profile using the same conversion parameters as those for the total scattering experimental data. In the PDF conversion process using the MaterialsPDF program, we subtracted the curved dummy profile from the experimental data as shown in **Fig. S15**. The intensity in the dummy profile is not significant but its effect on the profile at high-Q values is clear.

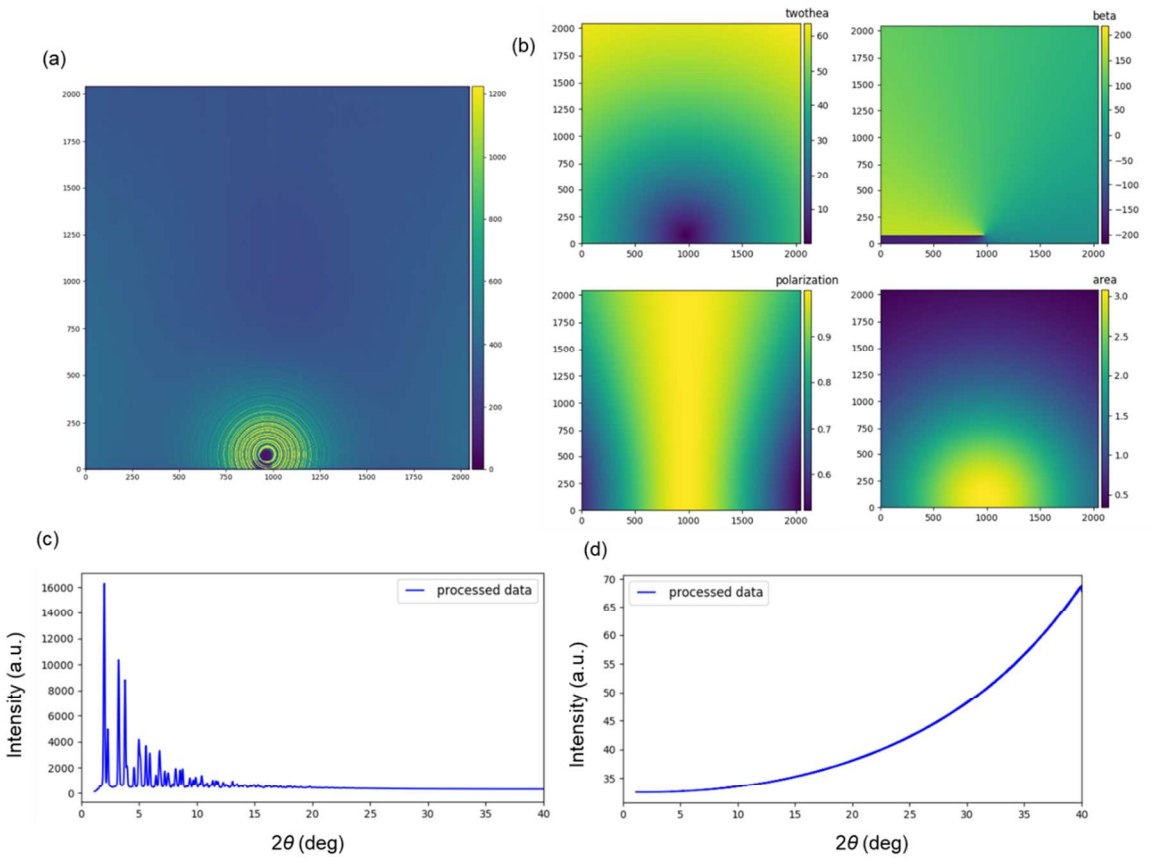

Figure S14 Example of data conversion. (a) Two-dimensional image data for CeO_2 after background subtraction. (b) Conversion parameters of each pixel. (c) Converted CeO_2 data. (d) Converted dummy data.

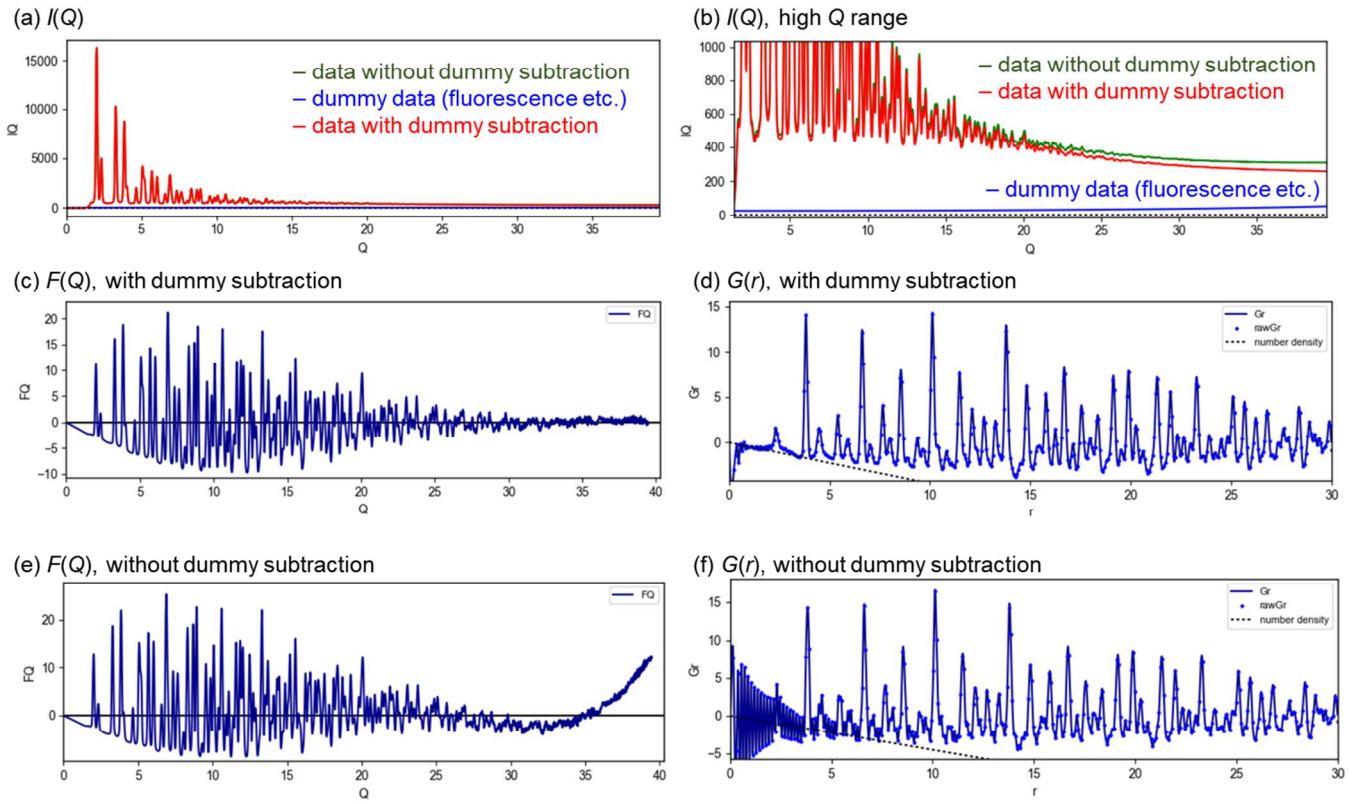

Figure S15 Example of data conversion from total scattering to reduced PDF, $G(r)$. (a, b) Total scattering patterns, $I(Q)$, for CeO_2. The dummy data is the profile obtained by converting the dummy image (100 counts on each pixel) into the 1D profile using the same parameters as those for the CeO_2 data. (c, d) Reduced structure function, $F(Q)$, and $G(r)$ obtained with dummy data correction. This is similar to fluorescence and dummy current correction. (e, f) $F(Q)$ and $G(r)$ without dummy data correction. The total scattering data was collected at BL08W of SPring-8 ($\lambda = 0.10790$ Å).

Conversion of 1D data into PDF using MaterialsPDF program

The data conversion from a 1D scattering profile to a PDF was performed using the MaterialsPDF program (**Fig. S16**). MaterialsPDF and PIXIA are parts of the Orochi program, with which X-ray scattering data can be seamlessly processed and analyzed on the same platform. "Orochi" is named after a legendary eight-headed dragon in Japanese mythology, "Yamata no Orochi". All the programs in Orochi are written in Python and connected to work concertedly. Thus, the data processed by the PIXIA program can be immediately handled in MaterialsPDF.

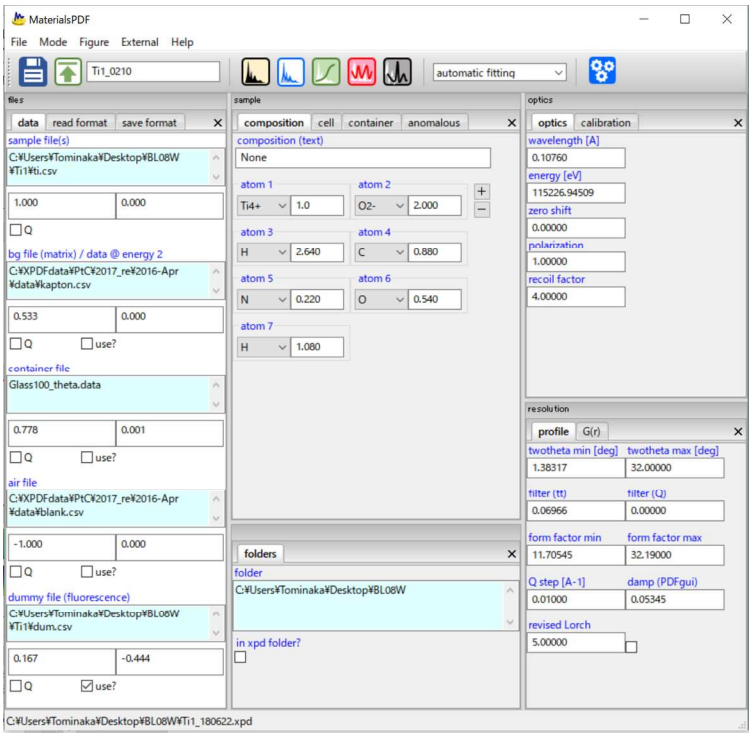

Figure S15 User interface of MaterialsPDF program.

The 1D profile for the CeO_2 data shown in **Fig. S14c** was treated in the MaterialsPDF program as shown in **Fig. S16**. This program was developed with reference to other programs, PDFgetX2,[3] PDFgetX3,[4] GudrunX[5] and a program used at BL04B2 at SPring-8 (which is written as a macro of Igor and used at the beamline). Most of the core equations are the same as those in PDFgetX2 and those in the book written by Egami and Billinge,[6] but other useful functions have also been added by referencing to other programs such as the revised Lorch function derived by Soper and Barney.[7]

Data is processed by background subtraction (or capillary and air intensity subtraction), fluorescence subtraction and Compton scattering subtraction by simulating the scattering profile based on the database to obtain the coherent scattering intensity, I_{coh},[8]

$$I_{\mathrm{coh}} = I_{\mathrm{cor}} - (I_{\mathrm{com}} + I_{\mathrm{flu}} + I_{\mathrm{bg}}), \qquad \text{(S1.3)}$$

where I_{com} is the Compton scattering intensity, I_{flu} is the fluorescence intensity, and I_{bg} is the background intensity. I_{bg} is often removed by subtracting the intensity obtained for a blank container. For the data processing of a 1D profile obtained by a 2D detector, the corrections of intensity using the profile obtained from a dummy image, as described in the previous sections are also very important as shown in **Fig. S15**.

Then, the data is normalized with a form factor based on the Faber–Ziman formalism calculated using atomic scattering factors[9-10] to obtain structure function, $S(Q)$,

$$S(Q) = \frac{I_{\mathrm{coh}} - NL(Q)}{N\langle f(Q)\rangle^2}, \qquad \text{(S1.4)}$$

$$L(Q) = \langle f(Q)^2\rangle - \langle f(Q)\rangle^2, \qquad \text{(S1.5)}$$

where $L(Q)$ is the Laue scattering term, N is the number of scattering atoms and $f(Q)$ is the atomic form factor. From the structural viewpoint, the Faber–Ziman structure function is a weighted sum of the structure function of each atom pair. From this structure function, the reduced PDF, $G(r)$, where r is the interatomic distance, can be derived through a Fourier transform, as

$$G(r) = \frac{2}{\pi}\int_{Q_{\mathrm{min}}}^{Q_{\mathrm{max}}} F(Q)\sin(Qr)\,dQ, \qquad \text{(S1.6)}$$

$$F(Q) = Q(S(Q) - 1), \qquad \text{(S1.7)}$$

where $F(Q)$ is named the reduced structure function.

In the MaterialsPDF program, these corrections can be performed as an interactive computation by checking the final PDF data. The obtained $G(r)$ is consistent with that obtained by other programs and can be well simulated (**Fig. S17**). We also verified the quality of $G(r)$ for SiO_2 glass as a standard amorphous material.

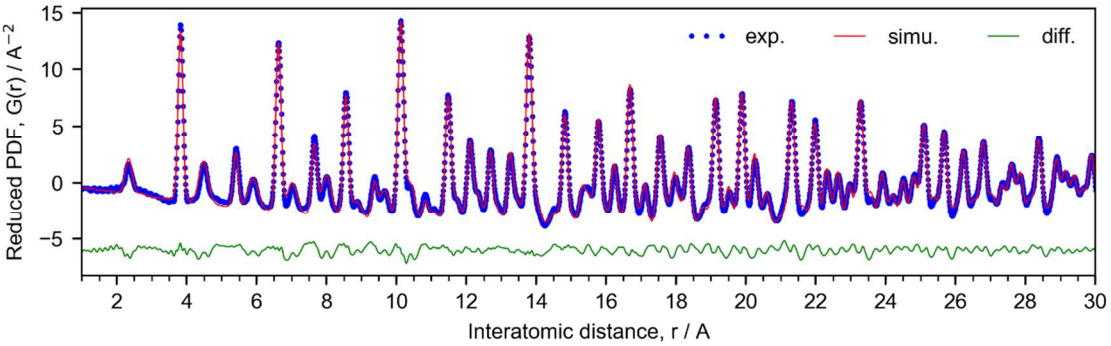

Figure S17 PDF fitting of CeO_2 (NIST 674B; a = 5.41165 Å) performed using PDFfit2 program (Q_{max} = 39.94 Å^{-1}, Q_{damp} = 0.05345). R_w = 11.8%.

Relative pair distribution functions (PDFs)

For the time-dependent PDFs, the concept of relative PDFs described below is useful for monitoring the change in structures because they can extract the change in PDFs rather than show entire PDFs. For example, in the reaction we investigated in this work, the solution contained precursors, reacted titanium oxide and solvent molecules. The structure of the solvent molecules can be regarded as constant at a given temperature. The change in structure is accounted for by the structural transformation from unreacted molecules to titanite. Thus, if we can normalize the data using the initial structure data, structure information related to the bulk solvent and the unreacted molecules can be cancelled. Then, it is easy to find the start of reactions.

The difference between two reduced PDFs having the same atomic concentrations and scattering factors can be expressed as follows.

$$\Delta G(r) = \frac{2}{\pi}\int_0^\infty \Delta F(Q)\sin(Qr)dQ \qquad \text{(S1.8)}$$

$$\Delta F(Q) = \frac{Q\Delta I_{\text{coh}}}{N\langle f(Q)\rangle^2} = \frac{Q\Delta I_{\text{tot}}}{N\langle f(Q)\rangle^2} \qquad \text{(S1.9)}$$

Assuming that PDFs obtained from multiple components can be approximated as the weighted sum of partials,[6] we can normalize the scattering data (I_{tot}) with $N\langle f\rangle^2$ for the changed components. Thus, the relative values $\Delta G(r)$ (or relative PDFs) are considered to be sensitive only to the changed components. However, the changed components change over time during in situ measurements and are difficult to know before detailed analyses; thus, we must assume or decide that the normalization function $N\langle f\rangle^2$ has reasonable values for the changing components. Therefore, the heights of the relative PDFs may not be accurate, although the interatomic distance information is still accurate and useful. Considering the use of spline curves as the normalization function in extended X-ray absorption fine structure (EXAFS) analysis, this relative PDF is similarly reliable.

Because of the simple calculations and possible cancellation of constant errors in the data, the computation of relative PDFs is an easy and straightforward way to determine the start of reactions. Thus, relative PDFs can be obtained at the time of time-resolved measurements and are useful for monitoring the reactions. The dimension and fundamental mathematics of such a relative PDF are similar to those of differential PDFs, but we refer to it as "relative" to emphasize the difference in the normalization.

Treatments of small-angle scattering peaks

The small-angle X-ray scattering intensities were excluded by defining a suitable minimum Q value (Q_{min}) as reported in the literature.[12] In more detail, Q_{min} = >1.0 $Å^{-1}$ was used for the titanate reactions, and this limit is sufficiently low to exclude the effect of particles of radius >5 Å.

Simulation of PDF using isolated cluster/nanosheet models

In the simulation with the removal of the baseline and using isolated cluster/nanosheet models, we first removed the baseline in the PDF by estimating it using equation (S1.14). The reduced PDF, $G(r)$, is expressed as follows:[6]

$$G(r) = 4\pi\rho_0(g(r) - 1), \qquad \text{(S1.10)}$$

where ρ_0 is the average number density and $g(r)$ is the atomic PDF. This function, $G(r)$, approaches the straight line of $-4\pi\rho_0 r$ as r approaches zero. According to the experimental data, $G(r)$ decays with increasing r owing to the limited resolution in Q and the limited atomic correlation associated with the particle size. For example, a Gaussian envelope of the following form is used in the PDFfit2 (and PDFfit) program:[13]

$$A(r) = exp\left(-\frac{(Q_{damp}r)^2}{2}\right), \qquad \text{(S1.11)}$$

where Q_{damp} is the damping constant. The spherical particle envelope is defined as follows:[14]

$$B(r,d) = \left(1 - \frac{3}{2}\frac{r}{d} + \frac{1}{2}\left(\frac{r}{d}\right)^3\right)H(d-r), \text{(S1.12)},$$

where d is the particle diameter and H is the Heaviside step function. Thus, the experimentally obtained reduced PDF of spherical particles can be expressed as

$$G_{\text{exp}}(r) = G(r)\cdot A(r)\cdot B(r,d) = 4\pi\rho_0\,(g(r)-1)\cdot A(r)\cdot B(r,d). \qquad \text{(S1.13)}$$

Thus, the baseline is $-4\pi\rho_0 r$ around $r = 0$ but it behaves as $-4\pi\rho_0 rAB$. Assuming that we can appropriately model the structure as well as the size effect, we can simulate the PDF well. However, this does not hold true for the structures we analyzed in this work. This is because the materials are clusters (too small to be simulated as spherical particles) and 2D (not spheres) and, moreover, the density associated with the surrounding solvent molecules is uncertain. Thus, we simulated the baseline of the PDFs using the following function:

$$C(r,d,x,s1,s2) = \begin{cases} 1 & (r<s1) \\ \dfrac{\left(1-\frac{3r}{2d}+\frac{1}{2}\left(\frac{r}{d}\right)^3\right)}{r^x}H(d-r) & (r>s2) \end{cases}, \qquad \text{(S1.14)}$$

where x is a constant used to adjust the decay curves, $s1$ is the upper limit where the particle size envelope cannot be held and $s2$ is the lower limit where the envelope can be held. This is an empirical model, and thus we will evaluate its physical meaning in order to optimize it. The range $s1 < r < s2$ was connected using a spline function.

This function is not definitive, but we consider that the structure analysis for clusters and nanosheets surrounded by solvent molecules requires a treatment removing such a baseline, and considering the uncertainty of the contribution of such a solvent to the baseline, our approach is still reasonable. Thus, we used this approach to obtain $4\pi\rho_0 g(r)A$, which can be simulated using the PDFfit program using a cluster or isolated nanosheet model as shown in **Fig. 5**, **Fig. 6** and **Fig. S10**.

References

1. Saito, K.; Tominaka, S.; Yoshihara, S.; Ohara, K.; Sugahara, Y.; Ide, Y., Room-Temperature Rutile TiO_2 Nanoparticle Formation on Protonated Layered Titanate for High-Performance Heterojunction Creation. *Acs Applied Materials & Interfaces* **2017,** *9* (29), 24538-24544.
2. Kahn, R.; Fourme, R.; Gadet, A.; Janin, J.; Dumas, C.; Andre, D., Macromolecular Crystallography with Synchrotron Radiation - Photographic Data-Collection and Polarization Correction. *J Appl Crystallogr* **1982,** *15* (Jun), 330-337.
3. Qiu, X.; Thompson, J. W.; Billinge, S. J. L., PDFgetX2: A GUI driven program to obtain the pair distribution function from X-ray powder diffraction data. *J. Appl. Cryst.* **2004,** *37*, 678.
4. Juhas, P.; Davis, T.; Farrow, C. L.; Billinge, S. J. L., PDFgetX3: a rapid and highly automatable program for processing powder diffraction data into total scattering pair distribution functions. *J Appl Crystallogr* **2013,** *46*, 560-566.
5. Soper, A. GudrunN and GudrunX: Programs for correcting raw neutron and x-ray total scattering data to differential cross section. https://www.isis.stfc.ac.uk/OtherFiles/Disordered%20Materials/Gudrun-Manual-2017-10.pdf.

6. Egami, T.; Billinge, S. J. L., *Underneath the Bragg peaks: structural analysis of complex materials*. Elsevier: Oxford, UK, 2003.
7. Soper, A. K.; Barney, E. R., Extracting the pair distribution function from white-beam X-ray total scattering data. *J Appl Crystallogr* **2011,** *44*, 714-726.
8. Brennan, S.; Cowan, P. L., A Suite of Programs for Calculating X-Ray Absorption, Reflection, and Diffraction Performance for a Variety of Materials at Arbitrary Wavelengths. *Rev Sci Instrum* **1992,** *63* (1), 850-853.
9. Waasmaier, D.; Kirfel, A., New Analytical Scattering-Factor Functions for Free Atoms and Ions. *Acta Crystallographica Section A* **1995,** *51*, 416-431.
10. Faber, T. E.; Ziman, J. M., A Theory of Electrical Properties of Liquid Metals .3. Resistivity of Binary Alloys. *Philos Mag* **1965,** *11* (109), 153-173.
11. Petkov, V.; Jeong, I. K.; Mohiuddin-Jacobs, F.; Proffen, T.; Billinge, S. J. L.; Dmowski, W., Local structure of In0.5Ga0.5As from joint high-resolution and differential pair distribution function analysis. *Journal of Applied Physics* **2000,** *88* (2), 665-672.
12. Farrow, C. L.; Billinge, S. J. L., Relationship between the atomic pair distribution function and small-angle scattering: implications for modeling of nanoparticles. *Acta Crystallogr A* **2009,** *65*, 232-239.
13. Farrow, C. L.; Juhas, P.; Liu, J. W.; Bryndin, D.; Bozin, E. S.; Bloch, J.; Proffen, T.; Billinge, S. J. L., PDFfit2 and PDFgui: computer programs for studying nanostructure in crystals. *Journal of Physics-Condensed Matter* **2007,** *19*, art. no. 335219.
14. Howell, R. C.; Proffen, T.; Conradson, S. D., Pair distribution function and structure factor of spherical particles. *Physical Review B* **2006,** *73*, art. no. 094107.

Structural information data

The followings are the structural information file exported from EXPO2014 (XRD data) and PDFgui (PDF fittings). Regarding the PDF fitting, the fittings were carried out under symmetry restraints though the exported structure ins *P*1 symmetry.

(A1) Crystalline product (Rietveld refinement, XRD)

```
_audit_creation_method           Expo2014

loop_
   _atom_type_symbol
   _atom_type_description
   _atom_type_scat_source
  'O'   'Oxygen'   'International Tables Vol C Tables 4.2.6.8 and 6.1.1.4'
  'Ti'   'Titanium'   'International Tables Vol C Tables 4.2.6.8 and 6.1.1.4'
  'H'   'Hydrogen'   'International Tables Vol C Tables 4.2.6.8 and 6.1.1.4'
  'C'   'Carbon'   'International Tables Vol C Tables 4.2.6.8 and 6.1.1.4'
  'N'   'Nitrogen'   'International Tables Vol C Tables 4.2.6.8 and 6.1.1.4'

_cell_length_a                    5.93882
_cell_length_b                    7.58785
_cell_length_c                   23.65053
_cell_angle_alpha                   90.000
_cell_angle_beta                  103.857
_cell_angle_gamma                   90.000
_cell_volume                     1034.745
_cell_measurement_temperature    298.3 K

_diffrn_ambient_temperature      298.3 K
_diffrn_radiation_wavelength     1.299000
_diffrn_radiation_type           Synchrtron

_symmetry_Int_Tables_number      3
_symmetry_cell_setting           monoclinic
_symmetry_space_group_name_H-M     'P 1 2 1'
_symmetry_space_group_name_hall    'P 2y'

loop_
  _symmetry_equiv_pos_site_id
  _symmetry_equiv_pos_as_xyz
  1   'x, y, z'
  2   '-x, y, -z'

loop_
  _atom_site_type_symbol
  _atom_site_label
  _atom_site_fract_x
  _atom_site_fract_y
  _atom_site_fract_z
  _atom_site_U_iso_or_equiv
  _atom_site_occupancy
```

_atom_site_adp_type

Ti	Ti1	0.9145	0.6295	0.7951	0.0046	1.0000 Uiso
Ti	Ti2	0.0855	0.3705	0.7049	0.0046	1.0000 Uiso
Ti	Ti3	0.4068	0.6270	0.7918	0.0046	1.0000 Uiso
Ti	Ti4	0.5932	0.3731	0.7082	0.0046	1.0000 Uiso
Ti	Ti5	0.4252	0.1242	0.7970	0.0046	1.0000 Uiso
Ti	Ti6	0.5748	0.8758	0.7030	0.0046	1.0000 Uiso
Ti	Ti7	0.9263	0.1174	0.7991	0.0046	1.0000 Uiso
Ti	Ti8	0.0737	0.8826	0.7009	0.0046	1.0000 Uiso
O	O1	0.8893	0.3681	0.7576	0.0080	1.0000 Uiso
O	O2	0.1107	0.6319	0.7424	0.0080	1.0000 Uiso
O	O3	0.1939	0.6252	0.8437	0.0080	1.0000 Uiso
O	O4	0.8061	0.3748	0.6563	0.0080	1.0000 Uiso
O	O5	0.3865	0.3756	0.7706	0.0080	1.0000 Uiso
O	O6	0.6135	0.6244	0.7294	0.0080	1.0000 Uiso
O	O7	0.6901	0.6253	0.8388	0.0080	1.0000 Uiso
O	O8	0.3099	0.3747	0.6612	0.0080	1.0000 Uiso
O	O9	0.9463	0.8863	0.9197	0.6119	1.0000 Uiso
O	O10	0.9463	1.1137	0.4197	0.6119	1.0000 Uiso
O	O11	0.4257	0.8776	0.7825	0.0080	1.0000 Uiso
O	O12	0.5277	0.1224	0.7156	0.0080	1.0000 Uiso
O	O13	0.7173	0.1253	0.8547	0.0080	1.0000 Uiso
O	O14	0.2827	0.8747	0.6453	0.0080	1.0000 Uiso
O	O15	0.8947	0.8803	0.7724	0.0080	1.0000 Uiso
O	O16	0.1052	0.1197	0.7276	0.0080	1.0000 Uiso
O	O17	0.2042	0.1250	0.8464	0.0080	1.0000 Uiso
O	O18	0.7958	0.8750	0.6536	0.0080	1.0000 Uiso
O	O19	0.5388	0.6302	0.5969	0.6119	1.0000 Uiso
O	O20	0.5388	0.3698	1.0969	0.6119	1.0000 Uiso
C	C1	0.8910	1.2599	1.0379	0.1089	1.0000 Uiso
C	C2	0.8910	0.7401	0.5379	0.1089	1.0000 Uiso
C	C3	0.1844	0.4890	1.0380	0.1089	1.0000 Uiso
C	C4	0.1844	1.5110	0.5380	0.1089	1.0000 Uiso
C	C5	0.3162	0.7599	0.9619	0.1089	1.0000 Uiso
C	C6	0.3162	1.2401	0.4619	0.1089	1.0000 Uiso
C	C7	0.6099	0.9890	0.9623	0.1089	1.0000 Uiso
C	C8	0.6099	1.0110	0.4623	0.1089	1.0000 Uiso
H	H1	0.8824	0.9840	0.9474	0.7343	1.0000 Uiso
H	H2	1.1382	0.8863	0.9308	0.7343	1.0000 Uiso
H	H3	1.0103	1.2114	0.3920	0.7343	1.0000 Uiso
H	H4	0.7545	1.1137	0.4086	0.7343	1.0000 Uiso
H	H5	0.4748	0.7279	0.6246	0.7343	1.0000 Uiso
H	H6	0.7307	0.6302	0.6080	0.7343	1.0000 Uiso
H	H7	0.6028	0.4675	1.0692	0.7343	1.0000 Uiso
H	H8	0.3469	0.3698	1.0858	0.7343	1.0000 Uiso
H	H9	0.9880	1.1292	1.0461	0.1307	1.0000 Uiso

H	H10	0.7028	1.2340	1.0153	0.1307	1.0000	Uiso
H	H11	0.8991	1.3292	1.0812	0.1307	1.0000	Uiso
H	H12	1.0238	0.7724	0.5798	0.1307	1.0000	Uiso
H	H13	0.7386	0.6675	0.5490	0.1307	1.0000	Uiso
H	H14	0.8275	0.8676	0.5138	0.1307	1.0000	Uiso
H	H15	0.2844	0.5622	1.0094	0.1307	1.0000	Uiso
H	H16	0.3082	0.4023	1.0704	0.1307	1.0000	Uiso
H	H17	0.0990	0.5885	1.0626	0.1307	1.0000	Uiso
H	H18	0.1529	1.3669	0.5246	0.1307	1.0000	Uiso
H	H19	0.1766	1.5269	0.5856	0.1307	1.0000	Uiso
H	H20	0.3621	1.5532	0.5324	0.1307	1.0000	Uiso
H	H21	0.3477	0.6158	0.9753	0.1307	1.0000	Uiso
H	H22	0.3245	0.7760	0.9143	0.1307	1.0000	Uiso
H	H23	0.1383	0.8019	0.9674	0.1307	1.0000	Uiso
H	H24	0.2159	1.3135	0.4904	0.1307	1.0000	Uiso
H	H25	0.1926	1.1533	0.4294	0.1307	1.0000	Uiso
H	H26	0.4020	1.3395	0.4373	0.1307	1.0000	Uiso
H	H27	0.4780	1.0210	0.9202	0.1307	1.0000	Uiso
H	H28	0.7630	0.9166	0.9515	0.1307	1.0000	Uiso
H	H29	0.6725	1.1167	0.9864	0.1307	1.0000	Uiso
H	H30	0.5126	0.8804	0.4539	0.1307	1.0000	Uiso
H	H31	0.7977	0.9848	0.4852	0.1307	1.0000	Uiso
H	H32	0.6031	1.0804	0.4190	0.1307	1.0000	Uiso
N	N1	0.5000	0.8744	1.0000	0.1089	1.0000	Uiso
N	N2	0.5000	1.1256	0.5000	0.1089	1.0000	Uiso
N	N3	0.0000	0.3744	1.0000	0.1089	1.0000	Uiso
N	N4	1.0000	0.6256	0.5000	0.1089	1.0000	Uiso

(A2) Crystalline product (PDF fitting)

```
_symmetry_space_group_name_H-M  'P1'
_symmetry_Int_Tables_number     1
_symmetry_cell_setting          triclinic

_cell_length_a                  5.94373
_cell_length_b                  7.57644
_cell_length_c                  23.5638
_cell_angle_alpha               90
_cell_angle_beta                103.333
_cell_angle_gamma               90

loop_
 _atom_site_label
 _atom_site_type_symbol
 _atom_site_fract_x
 _atom_site_fract_y
 _atom_site_fract_z
 _atom_site_U_iso_or_equiv
 _atom_site_adp_type
 _atom_site_occupancy
 Ti1  Ti   0.914500   0.629544   0.545080   0.004167 Uiso  1.0000
 Ti2  Ti   0.085500   0.629544   0.954920   0.004167 Uiso  1.0000
 Ti3  Ti   0.085500   0.370456   0.454920   0.004167 Uiso  1.0000
 Ti4  Ti   0.914500   0.370456   0.045080   0.004167 Uiso  1.0000
 Ti5  Ti   0.406773   0.626951   0.541853   0.004167 Uiso  1.0000
 Ti6  Ti   0.593227   0.626951   0.958147   0.004167 Uiso  1.0000
 Ti7  Ti   0.593227   0.373049   0.458147   0.004167 Uiso  1.0000
 Ti8  Ti   0.406773   0.373049   0.041853   0.004167 Uiso  1.0000
 Ti9  Ti   0.425198   0.124169   0.547055   0.004167 Uiso  1.0000
 Ti10 Ti   0.574802   0.124169   0.952945   0.004167 Uiso  1.0000
 Ti11 Ti   0.574802   0.875831   0.452945   0.004167 Uiso  1.0000
 Ti12 Ti   0.425198   0.875831   0.047055   0.004167 Uiso  1.0000
 Ti13 Ti   0.926259   0.117395   0.549096   0.004167 Uiso  1.0000
 Ti14 Ti   0.073741   0.117395   0.950904   0.004167 Uiso  1.0000
 Ti15 Ti   0.073741   0.882605   0.450904   0.004167 Uiso  1.0000
 Ti16 Ti   0.926259   0.882605   0.049097   0.004167 Uiso  1.0000
 O1   O    0.889348   0.368140   0.507591   0.008628 Uiso  1.0000
 O2   O    0.110652   0.368140   0.992409   0.008628 Uiso  1.0000
 O3   O    0.110652   0.631860   0.492409   0.008628 Uiso  1.0000
 O4   O    0.889348   0.631860   0.007591   0.008628 Uiso  1.0000
 O5   O    0.193907   0.625190   0.593688   0.008628 Uiso  1.0000
 O6   O    0.806093   0.625190   0.906312   0.008628 Uiso  1.0000
 O7   O    0.806093   0.374810   0.406312   0.008628 Uiso  1.0000
 O8   O    0.193907   0.374810   0.093688   0.008628 Uiso  1.0000
```

O9	O	0.386539	0.375560	0.520564	0.008628	Uiso	1.0000
O10	O	0.613461	0.375560	0.979436	0.008628	Uiso	1.0000
O11	O	0.613461	0.624440	0.479436	0.008628	Uiso	1.0000
O12	O	0.386539	0.624440	0.020564	0.008628	Uiso	1.0000
O13	O	0.690086	0.625340	0.588798	0.008628	Uiso	1.0000
O14	O	0.309914	0.625340	0.911202	0.008628	Uiso	1.0000
O15	O	0.309914	0.374660	0.411202	0.008628	Uiso	1.0000
O16	O	0.690086	0.374660	0.088798	0.008628	Uiso	1.0000
O17	O	0.946340	0.886310	0.669700	0.601406	Uiso	1.7372
O18	O	0.053660	0.886310	0.830300	0.601406	Uiso	1.7372
O19	O	0.053660	0.113690	0.330300	0.601406	Uiso	1.7372
O20	O	0.946340	0.113690	0.169700	0.601406	Uiso	1.7372
O21	O	0.425701	0.877620	0.532451	0.008628	Uiso	1.0000
O22	O	0.574299	0.877620	0.967549	0.008628	Uiso	1.0000
O23	O	0.617720	0.122380	0.465638	0.008628	Uiso	1.0000
O24	O	0.382280	0.122380	0.034362	0.008628	Uiso	1.0000
O25	O	0.717309	0.125340	0.604649	0.008628	Uiso	1.0000
O26	O	0.282691	0.125340	0.895351	0.008628	Uiso	1.0000
O27	O	0.282691	0.874660	0.395351	0.008628	Uiso	1.0000
O28	O	0.717309	0.874660	0.104649	0.008628	Uiso	1.0000
O29	O	0.894755	0.880340	0.522429	0.008628	Uiso	1.0000
O30	O	0.105245	0.880340	0.977571	0.008628	Uiso	1.0000
O31	O	0.105245	0.119660	0.477571	0.008628	Uiso	1.0000
O32	O	0.894755	0.119660	0.022429	0.008628	Uiso	1.0000
O33	O	0.204146	0.125000	0.596380	0.008628	Uiso	1.0000
O34	O	0.795854	0.125000	0.903620	0.008628	Uiso	1.0000
O35	O	0.795854	0.875000	0.403620	0.008628	Uiso	1.0000
O36	O	0.204146	0.875000	0.096380	0.008628	Uiso	1.0000
O37	O	0.538790	0.630190	0.346890	0.601406	Uiso	1.0000
O38	O	0.461210	0.630190	0.153110	0.601406	Uiso	1.0000
O39	O	0.461210	0.369810	0.653110	0.601406	Uiso	1.0000
O40	O	0.538790	0.369810	0.846890	0.601406	Uiso	1.0000
C1	C	0.891000	0.259900	0.787900	0.108974	Uiso	1.7372
C2	C	0.109000	0.259900	0.712100	0.108974	Uiso	1.7372
C3	C	0.109000	0.740100	0.212100	0.108974	Uiso	1.7372
C4	C	0.891000	0.740100	0.287900	0.108974	Uiso	1.7372
C5	C	0.184400	0.489000	0.788000	0.108974	Uiso	1.7372
C6	C	0.815600	0.489000	0.712000	0.108974	Uiso	1.7372
C7	C	0.815600	0.511000	0.212000	0.108974	Uiso	1.7372
C8	C	0.184400	0.511000	0.288000	0.108974	Uiso	1.7372
C9	C	0.316200	0.759900	0.711900	0.108974	Uiso	1.7372
C10	C	0.683800	0.759900	0.788100	0.108974	Uiso	1.7372
C11	C	0.683800	0.240100	0.288100	0.108974	Uiso	1.7372
C12	C	0.316200	0.240100	0.211900	0.108974	Uiso	1.7372
C13	C	0.609900	0.989000	0.712300	0.108974	Uiso	1.7372
C14	C	0.390100	0.989000	0.787700	0.108974	Uiso	1.7372

C15	C	0.390100	0.011000	0.287700	0.108974	Uiso	1.7372
C16	C	0.609900	0.011000	0.212300	0.108974	Uiso	1.7372
H1	H	0.882400	0.984010	0.697450	0.051872	Uiso	1.7372
H2	H	0.117600	0.984010	0.802550	0.051872	Uiso	1.7372
H3	H	0.117600	0.015990	0.302550	0.051872	Uiso	1.7372
H4	H	0.882400	0.015990	0.197450	0.051872	Uiso	1.7372
H5	H	0.138160	0.886310	0.680780	0.051872	Uiso	1.7372
H6	H	0.861840	0.886310	0.819220	0.051872	Uiso	1.7372
H7	H	0.861840	0.113690	0.319220	0.051872	Uiso	1.7372
H8	H	0.138160	0.113690	0.180780	0.051872	Uiso	1.7372
H9	H	0.474850	0.727890	0.374630	0.051872	Uiso	1.7372
H10	H	0.525150	0.727890	0.125370	0.051872	Uiso	1.7372
H11	H	0.525150	0.272110	0.625370	0.051872	Uiso	1.7372
H12	H	0.474850	0.272110	0.874630	0.051872	Uiso	1.7372
H13	H	0.730610	0.630190	0.357960	0.051872	Uiso	1.7372
H14	H	0.269390	0.630190	0.142040	0.051872	Uiso	1.7372
H15	H	0.269390	0.369810	0.642040	0.051872	Uiso	1.7372
H16	H	0.730610	0.369810	0.857960	0.051872	Uiso	1.7372
H17	H	0.988140	0.129210	0.796110	0.051872	Uiso	1.7372
H18	H	0.011860	0.129210	0.703890	0.051872	Uiso	1.7372
H19	H	0.011860	0.870790	0.203890	0.051872	Uiso	1.7372
H20	H	0.988140	0.870790	0.296110	0.051872	Uiso	1.7372
H21	H	0.703030	0.233850	0.765230	0.051872	Uiso	1.7372
H22	H	0.296970	0.233850	0.734770	0.051872	Uiso	1.7372
H23	H	0.296970	0.766150	0.234770	0.051872	Uiso	1.7372
H24	H	0.703030	0.766150	0.265230	0.051872	Uiso	1.7372
H25	H	0.898670	0.329280	0.831270	0.051872	Uiso	1.7372
H26	H	0.101330	0.329280	0.668730	0.051872	Uiso	1.7372
H27	H	0.101330	0.670720	0.168730	0.051872	Uiso	1.7372
H28	H	0.898670	0.670720	0.331270	0.051872	Uiso	1.7372
H29	H	0.284420	0.562240	0.759350	0.051872	Uiso	1.7372
H30	H	0.715580	0.562240	0.740650	0.051872	Uiso	1.7372
H31	H	0.715580	0.437760	0.240650	0.051872	Uiso	1.7372
H32	H	0.284420	0.437760	0.259350	0.051872	Uiso	1.7372
H33	H	0.308110	0.402220	0.820450	0.051872	Uiso	1.7372
H34	H	0.691890	0.402220	0.679550	0.051872	Uiso	1.7372
H35	H	0.691890	0.597780	0.179550	0.051872	Uiso	1.7372
H36	H	0.308110	0.597780	0.320450	0.051872	Uiso	1.7372
H37	H	0.099070	0.588550	0.812720	0.051872	Uiso	1.7372
H38	H	0.900930	0.588550	0.687280	0.051872	Uiso	1.7372
H39	H	0.900930	0.411450	0.187280	0.051872	Uiso	1.7372
H40	H	0.099070	0.411450	0.312720	0.051872	Uiso	1.7372
H41	H	0.347680	0.615750	0.725300	0.051872	Uiso	1.7372
H42	H	0.652320	0.615750	0.774700	0.051872	Uiso	1.7372
H43	H	0.652320	0.384250	0.274700	0.051872	Uiso	1.7372
H44	H	0.347680	0.384250	0.225300	0.051872	Uiso	1.7372

H45	H	0.324440	0.775990	0.664270	0.051872	Uiso	1.7372
H46	H	0.675560	0.775990	0.835730	0.051872	Uiso	1.7372
H47	H	0.675560	0.224010	0.335730	0.051872	Uiso	1.7372
H48	H	0.324440	0.224010	0.164270	0.051872	Uiso	1.7372
H49	H	0.138390	0.801930	0.717500	0.051872	Uiso	1.7372
H50	H	0.861610	0.801930	0.782500	0.051872	Uiso	1.7372
H51	H	0.861610	0.198070	0.282500	0.051872	Uiso	1.7372
H52	H	0.138390	0.198070	0.217500	0.051872	Uiso	1.7372
H53	H	0.478210	0.020920	0.670180	0.051872	Uiso	1.7372
H54	H	0.521790	0.020920	0.829820	0.051872	Uiso	1.7372
H55	H	0.521790	0.979080	0.329820	0.051872	Uiso	1.7372
H56	H	0.478210	0.979080	0.170180	0.051872	Uiso	1.7372
H57	H	0.763200	0.916750	0.701540	0.051872	Uiso	1.7372
H58	H	0.236800	0.916750	0.798460	0.051872	Uiso	1.7372
H59	H	0.236800	0.083250	0.298460	0.051872	Uiso	1.7372
H60	H	0.763200	0.083250	0.201540	0.051872	Uiso	1.7372
H61	H	0.672130	0.116760	0.736420	0.051872	Uiso	1.7372
H62	H	0.327870	0.116760	0.763580	0.051872	Uiso	1.7372
H63	H	0.327870	0.883240	0.263580	0.051872	Uiso	1.7372
H64	H	0.672130	0.883240	0.236420	0.051872	Uiso	1.7372
N1	N	0.500000	0.874400	0.750000	0.108974	Uiso	1.7372
N2	N	0.500000	0.125600	0.250000	0.108974	Uiso	1.7372
N3	N	0.000000	0.374400	0.750000	0.108974	Uiso	1.7372
N4	N	0.000000	0.625600	0.250000	0.108974	Uiso	1.7372

(A3) Titanate in the solution after 480 min thermal treatment and then cooled (PDF fitting)

```
_symmetry_space_group_name_H-M  'P1'
_symmetry_Int_Tables_number     1
_symmetry_cell_setting          triclinic

_cell_length_a                  2.98708
_cell_length_b                  3.80296
_cell_length_c                  100
_cell_angle_alpha               90
_cell_angle_beta                90
_cell_angle_gamma               90

loop_
 _atom_site_label
 _atom_site_type_symbol
 _atom_site_fract_x
 _atom_site_fract_y
 _atom_site_fract_z
 _atom_site_U_iso_or_equiv
 _atom_site_adp_type
 _atom_site_occupancy
 Ti1  Ti   0.500000   0.000000   0.510621   0.006507 Uani  1.0000
 Ti2  Ti   0.000000   0.500000   0.489379   0.006507 Uani  1.0000
 O1   O    0.500000   0.500000   0.501717   0.018110 Uani  1.0000
 O2   O    0.000000   0.000000   0.498283   0.018110 Uani  1.0000
 O3   O    0.000000   0.000000   0.521722   0.022041 Uani  1.0000
 O4   O    0.500000   0.500000   0.478278   0.022041 Uani  1.0000
loop_
 _atom_site_aniso_label
 _atom_site_aniso_U_11
 _atom_site_aniso_U_22
 _atom_site_aniso_U_33
 _atom_site_aniso_U_12
 _atom_site_aniso_U_13
 _atom_site_aniso_U_23
 Ti1   0.006508  0.005991  0.007021  0.000000  0.000000  0.000000
 Ti2   0.006508  0.005991  0.007021  0.000000  0.000000  0.000000
 O1    0.014201  0.011963  0.028166  0.000000  0.000000  0.000000
 O2    0.014201  0.011963  0.028166  0.000000  0.000000  0.000000
 O3    0.020744  0.023316  0.022063  0.000000  0.000000  0.000000
 O4    0.020744  0.023316  0.022063  0.000000  0.000000  0.000000
```

(A3) Titanate in the solution before thermal treatment measured at RT (PDF fitting)

```
_cell_length_a                    6.16927
_cell_length_b                    7.68268
_cell_length_c                   95.00000
_cell_angle_alpha                   90
_cell_angle_beta                    90
_cell_angle_gamma                     90
_space_group_name_H-M_alt           'P 1'
_space_group_IT_number              1

loop_
_space_group_symop_operation_xyz
  'x, y, z'

loop_
  _atom_site_label
  _atom_site_occupancy
  _atom_site_fract_x
  _atom_site_fract_y
  _atom_site_fract_z
  _atom_site_adp_type
  _atom_site_U_iso_or_equiv
  _atom_site_type_symbol
  Ti1      1.0    0.105826     0.092959     0.509817    Uiso  0.002099 Ti
  Ti2      1.0    0.109506     0.668363     0.510872    Uiso  0.002099 Ti
  Ti3      1.0    0.624933     0.113107     0.511611    Uiso  0.002099 Ti
  Ti4      1.0    0.626051     0.662638     0.511862    Uiso  0.002099 Ti
  Ti5      1.0    0.374600     0.335317     0.489627    Uiso  0.002099 Ti
  Ti6      1.0    0.374803     0.906978     0.488793    Uiso  0.002099 Ti
  Ti7      1.0    0.875149     0.396816     0.491718    Uiso  0.002099 Ti
  Ti8      1.0    0.872007     0.914820     0.487852    Uiso  0.002099 Ti
  O1       1.0    0.176504     0.385357     0.507185    Uiso  0.002000 O
  O2       1.0    0.124612     0.860770     0.500442    Uiso  0.002000 O
  O3       1.0    0.598670     0.388126     0.504968    Uiso  0.002000 O
  O4       1.0    0.638452     0.870962     0.501049    Uiso  0.002000 O
  O5       1.0    0.375706     0.122116     0.499525    Uiso  0.002000 O
  O6       1.0    0.380203     0.624687     0.497117    Uiso  0.002000 O
  O7       1.0    0.844170     0.151153     0.497009    Uiso  0.002000 O
  O8       1.0    0.803767     0.654447     0.494035    Uiso  0.002000 O
  O9       1.0    0.375000     0.110029     0.521669    Uiso  0.002000 O
  O10      1.0    0.375000     0.610029     0.521669    Uiso  0.002000 O
  O11      1.0    0.875000     0.110029     0.521669    Uiso  0.002000 O
  O12      1.0    0.878286     0.612221     0.521678    Uiso  0.002000 O
  O13      1.0    0.142021     0.397028     0.478038    Uiso  0.002000 O
  O14      1.0    0.125000     0.889971     0.478331    Uiso  0.002000 O
```

O15	1.0	0.625000	0.389971	0.478331	Uiso	0.002000	O
O16	1.0	0.619299	0.878863	0.478454	Uiso	0.002000	O